Natural history of experimental intracerebral hemorrhage: sonography, computed tomography and neuropathology.

D R Enzmann, R H Britt, B E Lyons, J L Buxton and D A Wilson

AJNR Am J Neuroradiol 1981, 2 (6) 517-526
http://www.ajnr.org/content/2/6/517

Natural History of Experimental Intracerebral Hemorrhage: Sonography, Computed Tomography and Neuropathology

D. R. Enzmann[1]
R. H. Britt[2]
B. E. Lyons[2]
J. L. Buxton[3]
D. A. Wilson[3]

The evolution of intracerebral hemorrhage was investigated in a canine model by high resolution sonography, computed tomography (CT), and neuropathologic examination. In 12 dogs, a parietal lobe hematoma was introduced by craniotomy. The sonographic appearance of acute hemorrhage was characteristic and consisted of a sharply circumscribed, homogeneous, highly echogenic lesion, the size and shape of which correlated closely to the area of increased density seen on the CT scan. This changed within 3–4 days to an echogenic rim surrounding a hypoechoic center. Histologically, this change corresponded to a loss of integrity of individual red blood cells. This occurred earliest in the hemorrhage center causing a hypoechoic center, while intact red blood cells at the periphery accounted for the echogenic rim. Shortly after the red blood cells lost their biconcave shape they began to lose their hemoglobin causing the hemorrhage to become isodense with surrounding brain on the CT scan. Faint contrast enhancement by CT was noted at this early stage and was related primarily to a mononuclear perivascular infiltrate at the edge of the hemorrhage. A collagen capsule formed around the hemorrhage over a 2 week period. This capsule slowly replaced intact red cells as the cause of the now shrinking echogenic rim. This capsule was also responsible for the increasing ring contrast enhancement around the resolving hemorrhage. The sequence of image changes seen on both CT and sonography in this experimental model closely resembled the findings seen in intracerebral hemorrhage in patients.

Continued refinement of sonographic equipment has expanded its role in the investigation of intracranial disease. Echoencephalography of the neonate is an accepted and expanding diagnostic modality [1–3]. In our clinical investigation of subependymal germinal matrix and intraventricular hemorrhages in premature infants, we observed a changing, evolving sonographic appearance of the parenchymal component of these hemorrhages. We sought to investigate the mechanism of these changes in an experimental model of intracerebral hemorrhage by correlating the high resolution sonograms with concurrent computed tomographic (CT) scans and concomitant neuropathologic findings.

Materials and Methods

Serial imaging using both high resolution sonograms and CT brain scans was performed in an experimental model of intracerebral hemorrhage in mongrel dogs. The intracerebral hematoma was produced in the parietal lobe in the following manner: Dogs were sedated with acepromazine maleate (10 mg/5 kg, intramuscularly), anesthetized with intravenous sodium phenobarbital (16 mg/2.5 kg), and intubated with an endotracheal tube. The dog's head was affixed to a stereotactic device and a midline scalp incision was made to reflect the temporalis muscle and expose the frontoparietal skull. A 3 × 5 cm craniotomy was performed to provide a window for admitting the entire sound beam of the sonographic probe. A 25 gauge needle was used to inject freshly drawn venous blood into the parietal lobe to a depth of 3–4 mm from the surface; the blood volume was 1–3 ml. The operative site was vigorously flushed with saline and closed in layers. Sterile technique was main-

Received February 27, 1981; accepted after revision July 9, 1981.

Presented at the annual meeting of the American Society of Neuroradiology, Chicago, IL, April 1981.

This work was supported by a Department of Radiology research grant and National Institutes of Health grant 1 R01 DS 16404–01.

[1] Department of Radiology, Stanford University School of Medicine, Stanford, CA 54305. Address reprint requests to D. R. Enzmann.

[2] Department of Neurosurgery, Stanford University School of Medicine, Stanford, CA 94305.

[3] Stanford Research Institute International, Stanford, CA 94305.

AJNR 2:517–526, November/December 1981
0195–6108/81/0206–0517 $00.00

tained throughout the procedure.

High resolution sonographic and CT imaging studies were performed in a serial manner in each dog up to the day of sacrifice. Sonograms were obtained at about 3–4 day intervals, and the following days were represented: 1–4, 6, 8, 9, 13, 16, and 20. CT brain scans were obtained at about 5 day intervals and days 1–4, 6, 8, 9, 13, 16, and 20 were included. A total of 43 sonograms and 30 CT scans were obtained in 12 dogs. CT scans were always accompanied by concurrent high resolution sonograms; the additional sonograms were obtained at intervals between CT scans.

Imaging Techniques

High resolution sonograms of the experimental hemorrhage were obtained through the scalp muscles overlying the craniotomy defect in both coronal and sagittal planes. Scans on day 1 were obtained immediately after surgery while the dog was still under anesthesia. Subsequent sonograms were obtained under sedation unless a CT scan was planned for the same day, in which case the dog was anesthetized for both studies. For sonography, a real time B scanner was used with a 10 MHz, 64 element linear array. Dynamic focusing was used in both transmit and receive to provide submillimeter resolution in both dimensions over the entire image. A fixed acoustical lens provided focusing in the direction orthogonal to the image plane. The field of view was 3 cm wide × 4 cm deep; images were generated at 30 frames/sec. Freeze-frame images were recorded on Polaroid film.

CT brain scans were obtained in the coronal projection on a General Electric 8800 body scanning unit using the following factors: 120 kVp, 320 mA, 3.3 msec pulse width, and 5 mm section thickness. The dogs were scanned in a prone position at 5 mm intervals through the brain to delineate the entire extent of the hemorrhage. Once the lesion was delineated the maximal area of hemorrhage was chosen and serial scans were obtained at this level after intravenous contrast medium (66% diatrizoate megalumine and 10% diatrizoate sodium [Renografin 76, Squibb, Princeton, N.J.] 4 ml/kg) was injected by hand in a rapid bolus. Sequential coronal CT scans were obtained at this site at the following intervals: (1) immediately after the bolus injection (0 min); (2) 5 min; (3) 10 min; (4) 15 min; and (5) 30 min. Precontrast CT attenuation values of the density of the hematoma were determined at various time intervals using the region of interest capability on the display console. In the same manner attenuation values of contrast enhancement and its time course over 30 min were determined at the various stages of hematoma resolution. A region of interest in the parietal lobe in the unaffected hemisphere was used as baseline brain attenuation to determine the magnitude of contrast enhancement. This baseline brain attenuation value was obtained for each dog at each CT scanning session to provide an internal control.

Neuropathologic Evaluation

The histopathology of the hematomas was studied by sacrificing dogs at different time intervals after hemorrhage production. Neuropathologic correlation was available for days 1–4, 6–8, 10, 13, 16, and 21 after hemorrhage. After sacrifice, the entire dog's brain was removed and immediately placed in 4% formaldehyde for at least 5 weeks. These 12 brains were then cut into 0.5 cm coronal slices and photographed for comparison with the high resolution sonograms and CT scans. Sections that encompassed the entire hemorrhage were cut and processed. The hematoxylin and eosin (H and E) stain was used to evaluate the general cytologic features of hematoma resolution. Reticulin, hematoxylin van Giesen, and Masson trichrome stains were used to evaluate capsule formation and final organization of the hematoma. Glial fibrillary acidic protein was used to detect the presence of reactive astrocytes and gliosis. The hemoglobin and hemosiderin stain was used to follow the breakdown of hemoglobin into hemosiderin pigment.

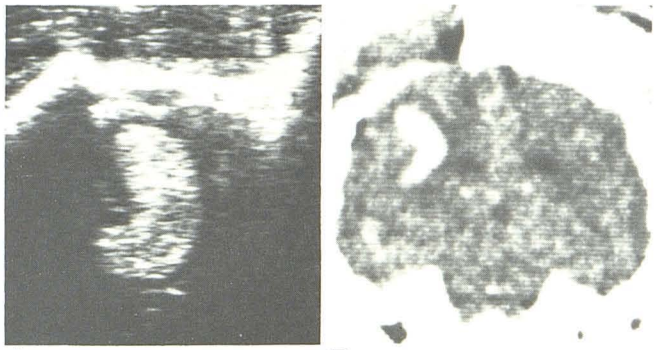

Fig. 1.—Acute hemorrhage, day of surgery. **A**, High resolution sonogram in coronal plane. Sharply marginated, lesion comprised of homogeneous echoes. Surrounding brain was hypoechoic. Horizontal echogenic band above hemorrhage represents craniotomy defect and dura. **B**, Coronal CT scan. High attenuation lesion of similar, size, shape, and orientation. Low attenuation halo around hemorrhage was cerebral edema not seen on **A**. Small amount of blood in right temporal horn.

Results

The high resolution sonograms correlated closely with CT and neuropathologic findings. The sonogram accurately delineated the size, shape, and position of the hemorrhage and gave an indication of the microscopic pathologic changes. Although CT, sonographic, and pathologic changes showed gradual changes as the intracerebral hemorrhage resolved, we divided the process into four stages based on histologic criteria. These stages highlight important changes and clarify the imaging and pathologic correlations. The stages in our model were: acute (days 1–3); subacute (days 4–8); capsule (days 9–13); and organization (days 13 and after).

In the acute stage, the hemorrhage was homogeneous, highly echogenic, and sharply circumscribed on the sonogram (figs. 1, 3, and 4). The size and shape of this echogenic area correlated very closely with the size and shape of the area of increased attenuation seen on the CT scan (fig. 1). Both of these imaging techniques accurately delineated the gross neuropathologic appearance of the hemorrhage. The region of homogeneous echoes, as well as the area of increased attenuation on CT, corresponded to the microscopic finding of tightly packed, intact red blood cells composing the hematoma. In the acute stage, a halo of low density was seen in the CT scan around the high density hemorrhage, but a comparable region could not be identified on the sonogram. The neuropathologic counterpart of this low density halo was caused by cerebral edema in adjacent white matter (fig. 2A). A thin band of acellular proteinaceous fluid at the interface of the hemorrhage and surrounding brain may have contributed to this halo (fig. 2B). During this stage the red blood cells of the hematoma were largely

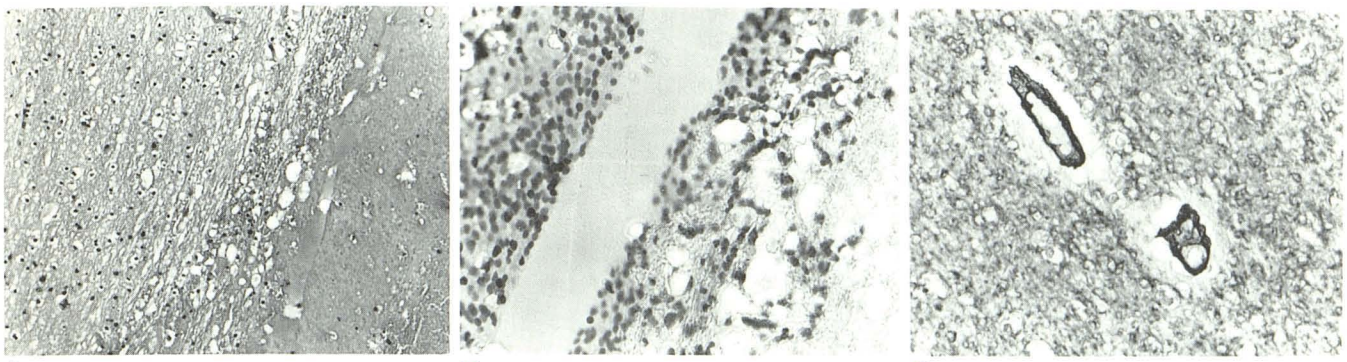

A B C

Fig. 2.—Acute hemorrhage, day 2. **A**, Very mild inflammatory infiltrate surrounds hematoma. Edema in surrounding white matter (left side of image) was extensive (H and E ×190). **B**, At periphery of hematoma. Acellular zone of plasma separates surrounding brain from red blood cell mass (hemoglobin and hemosiderin ×480). **C**, Acute hematoma stage. Reticulin stain (dark circular areas) ×480. Neither neovascularity nor sprouting of precollagen precursors.

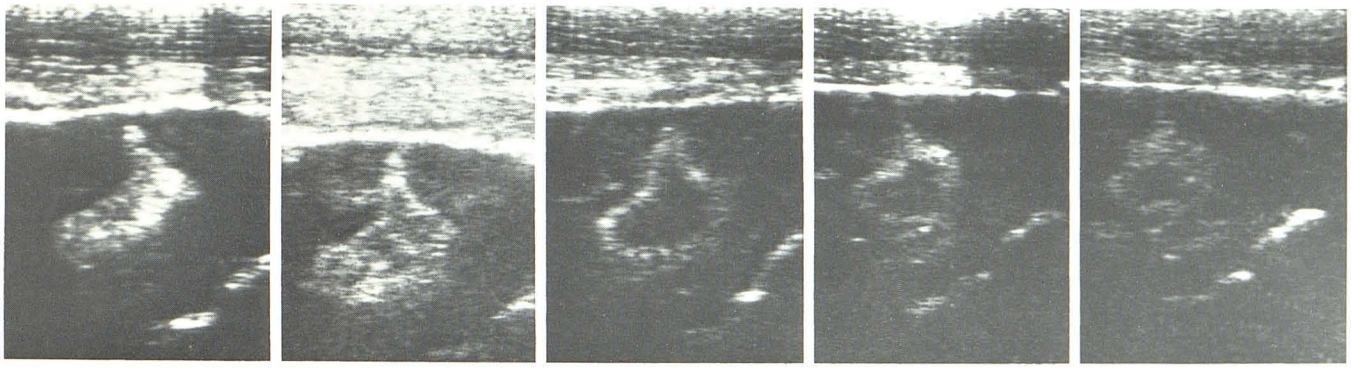

A B C D E

Fig. 3.—Resolving hemorrhages, days 1–16. Serial sagittal high resolution sonograms. **A**, Day 1. Typical well defined echogenic lesion. **B**, Late acute stage, day 3. Some inhomogeneity of echoes in center heralds hypoechoic center–echogenic rim appearance of subacute stage, day 9 (**C**). **C–E**, Hemorrhage progressiveiy diminished. **D**, Capsule stage, day 13. Thickened rim persisted through organization stage, day 16, (**E**). Intensity of echoes gradually decreased (**D** and **E**) as neovascularity and collagen became more responsible for echoes compared with red blood cells in early stages (**A** and **B**). Oblique echogenic band in lower right hand corner of images was choroid plexus.

intact but progressive crenation was seen over the first 3 days. A mild inflammatory reaction in the adventitial sheaths of vessels surrounded the hematoma at this time (fig. 2A). We termed this perivascular cuffing *cerebritis.* The inflammatory infiltrate consisted primarily of small lymphocytes and large mononuclear cells with only a few, scattered polymorphonuclear leukocytes. The cerebritis was very focal around the hematoma. Reticulin stain showed no evidence of reticulin or neovascularity (fig. 2C). A narrow zone of infarction with death of neurons surrounded the hematoma and was associated with significant edema of the white matter.

The hemorrhage began to change its sonographic appearance in the late acute and subacute stages (figs. 3 and 4). The homogeneous echoes became inhomogeneous. This inhomogeneity increased rapidly with the echoes in the center of the hemorrhage and faded more rapidly than those at the periphery, resulting in an image with an echogenic rim and a hypoechoic center (fig. 4). This change reflected microscopic changes involving primarily the integrity of the red blood cells. Red blood cells became progressively more crenated and lysed (fig. 5A). They lost their biconcave configuration and acquired a more amorphous shape that resulted in tighter packing of degenerating cells. The high resolution sonogram was very sensitive to this change, exhibiting fewer echoes as the red blood cells lost their distinctive shape and ruptured. In addition, the proteinaceous cell contents from cell rupture filled the spaces between remaining intact cells. Collections of plasma among the tightly packed red blood cells contributed to the increasing inhomogeneity of echoes (fig. 5B). These changes in red blood cell integrity and cell-to-cell relations developed first in the hemorrhage center and persisted through the subacute stage. As these changes occurred, the attenuation values of the hemorrhage on the CT scan decreased becoming isodense with surrounding brain. At the isodense stage by CT, the echogenic rim with hypoechoic center pattern was well established on the sonogram (fig. 4). Hemoglobin was identified within red blood cells early in this stage. Soon after the red blood cells lost their distinctive biconcave

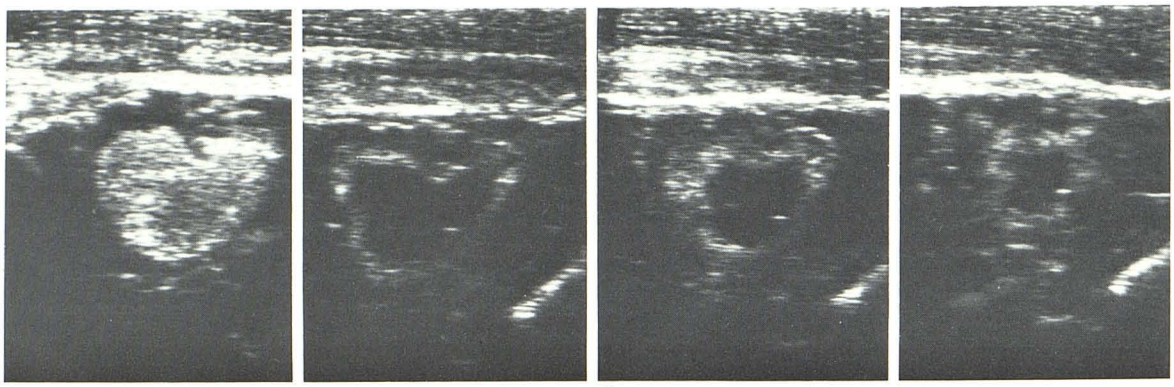

Fig. 4.—Resolving hemorrhage, days 1–13. Sagittal high resolution sonograms. **A**, Acute hemorrhage, day 1. Sharply circumscribed and homogeneously echogenic. Brain around hemorrhage was hypoechoic; cerebral edema was not detected. **B**, Subacute hemorrhage, day 5. Hypoechoic center surrounded by thin, echogenic rim. Rim was caused by intact red blood cells periphery of hemorrhage, the central red blood cells having lysed. Surrounding brain remained hypoechoic. Capsule stage, days 9 (**C**) and 13 (**D**). Hypoechoic center–echogenic rim persisted although rim was now thicker, especially on cortical side. Surrounding brain began to show some patchy areas of echogenicity around main hemorrhage. Echoes both in rim and in surrounding brain were related to neovascularity and associated collagen fibers. Thickness of the rim increased while hemorrhage as a whole diminished (**C** and **D**). Echoes around resolving hemorrhage increased with further resolution. Oblique band of echoes in lower right hand corner of images was choroid plexus in lateral ventricle.

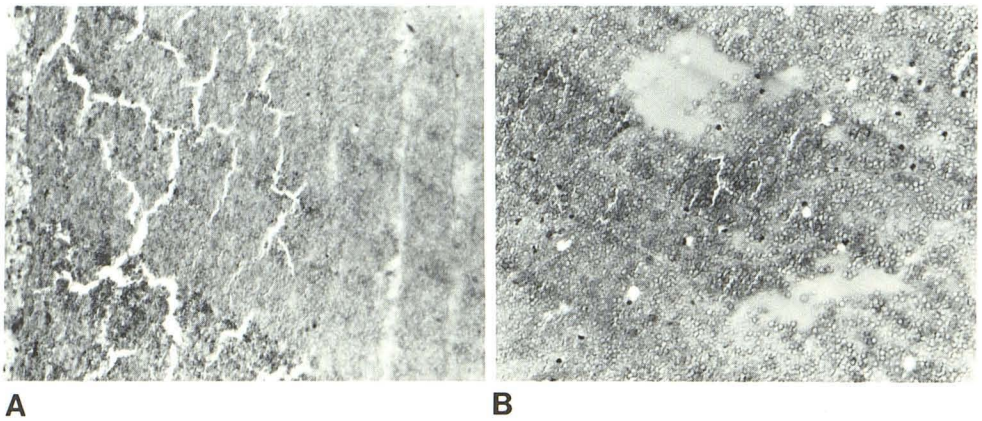

Fig. 5.—Subacute hemorrhage, day 4. **A**, Large areas of "ghost" red blood cells in center of hematoma (right side) with more intact red blood cells at periphery (trichrome × 190). **B**, Scattered pools of plasma separated within core of hematoma (trichrome ×300).

shape, hemoglobin could no longer be identified within them. The red blood cells lost their echogenicity before they lost their hemoglobin and hence their density on the CT scan. The decreased density of the hemorrhage on CT correlated closely with the loss of hemoglobin and the appearance of ghost cells. The conversion of hemoglobin into hemosiderin was first seen in macrophages on day 8. The hemosiderin-stained macrophages were seen both in the hematoma and at its edge (fig. 6A).

Cerebritis of the surrounding brain began in the acute stage and progressively increased and reached its maximum during the subacute stage (fig. 6B). Large foamy macrophages and fibroblasts appeared on the edge of the hematoma (fig. 6A). By day 4 the reticulin stain showed the presence of some neovascularity, which increased with time (figs. 6C and 6D). By day 8 reticulin was bridging some of the vessels (fig. 6D). Mature collagen was seen late in this stage around a few vessels. Edema of the white matter reached its peak early in this stage but started to decrease by day 7. Reactive astrocytes appeared in the surrounding brain at the end of this stage.

As the hemorrhage evolved further, it began to diminish in the capsule stage, but it retained the features of a hypoechoic center and echogenic rim (figs. 3 and 4). The echoes were now produced by a collagen-macrophage network rather than by red blood cells. Although the echoes were more numerous, they became less intense. The rim of echoes thickened as the lesion diminished (figs. 3 and 4). Thickening of the rim correlated best with formation of a capsule composed of increased numbers of collagen and reticulin fibers deposited around proliferating neovascularity (figs. 7A–7C). The echogenic rim became less uniform in thickness, showing projections of echoes emanating from it; these represented clusters of neovascularity (figs. 3 and 4). Wall formation was more extensive and more complete on the cortical side of the hemorrhage than on the ventricular side. Scattered intact red blood cells were still identified at the periphery of the hematoma but contributed little to the

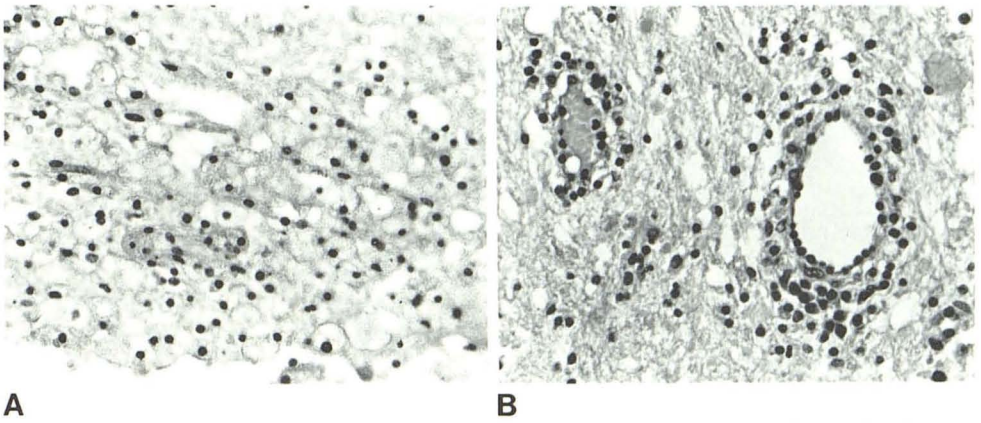

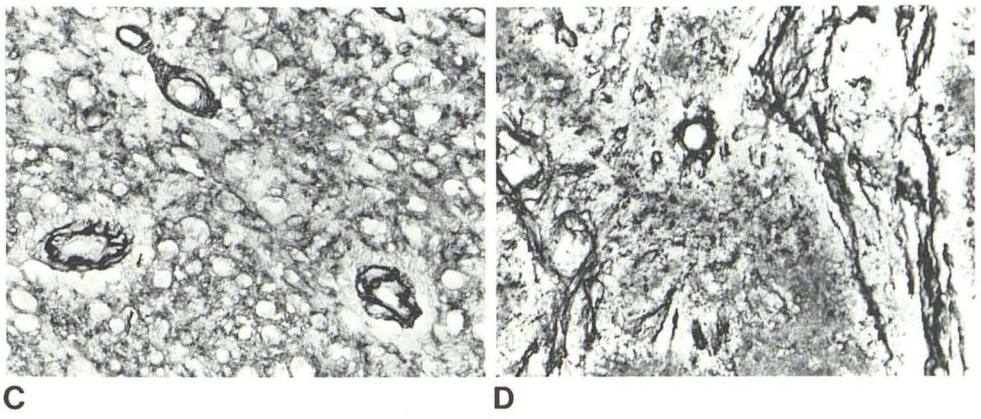

Fig. 6.—Subacute hemorrhage. **A**, At edge of hematoma, fibroblasts (spindle-shaped cells) and large foamy macrophages line edge of hematoma in 8-day-old lesion (H and E ×480). **B**, Cerebritis, defined as periadventitial infiltration of inflammatory cells, reached maximum degree by day 6 (H and E ×480). Mononuclear cells predominated. **C**, Early suggestion of reticulin sprouting from edges of existing blood vessels by day 4. Neovascularity started to increase. Extensive white matter edema (Reticulin ×480). **D**, By day 8, reticulin was bridging space between vessels indicating earliest evidence of capsule formation (reticulin ×480).

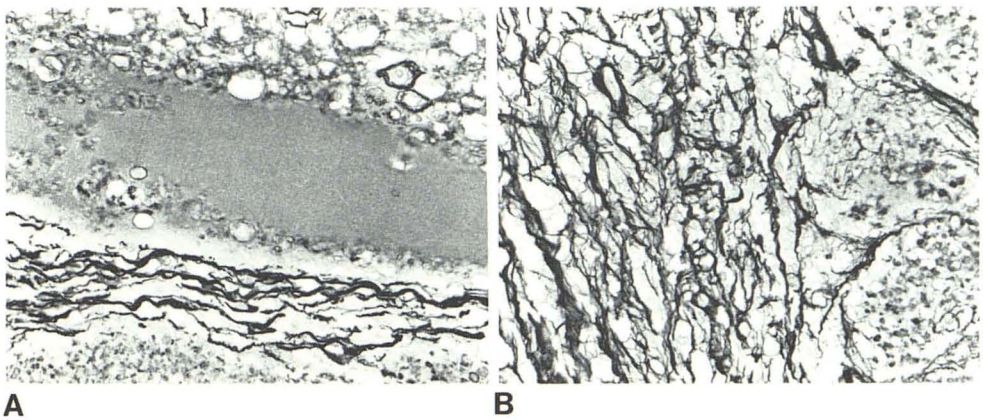

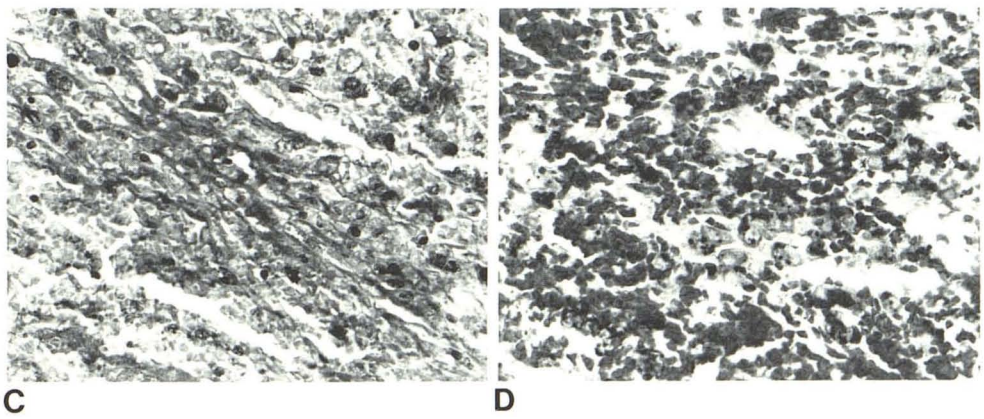

Fig. 7.—Capsule stage of hemorrhage. **A** and **B**, days 9–13. Capsule forms around resolving hematoma (reticulin ×480). Thin layer of plasma separates reticulin from hemorrhage on less well developed ventricular side (**A**). On opposite cortical side of lesion, extensive reticulin deposition was already present (**B**). **C**, Day 10 hemorrhage. Collagen fibers and fibroblasts formed an early capsule. (trichrome ×480). **D**, Macrophages in center of resolving hematoma, but hemosiderin (dark staining dots within cells) seen in only small amounts at this stage of hematoma resolution (hemoglobin and hemosiderin ×480).

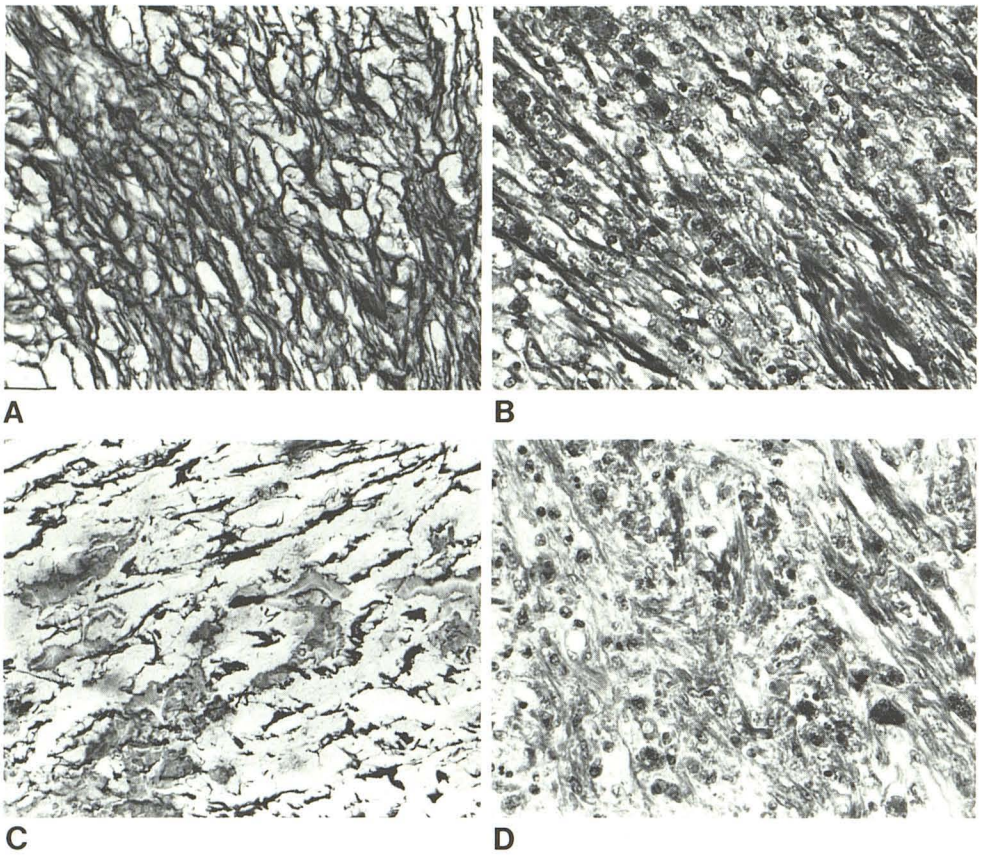

Fig. 8.—Organization stage of hemorrhage. **A** and **B**, Capsule was characterized by multiple parallel bundles of fibers of reticulin (**A**, ×480) and collagen (**B**, trichrome × 480). In contrast, organization of hematoma center characterized by more random and disorganized pattern of reticulin (**C**, ×480) and collagen (**D**, trichrome ×480) deposition.

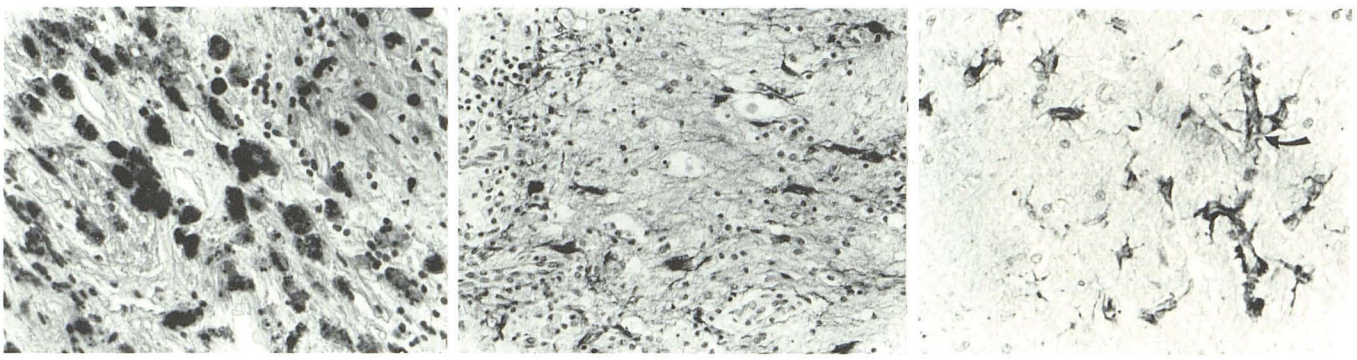

Fig. 9.—Organization stage of hemorrhage, day 21. **A**, Numerous macrophages in organizing central part of hematoma were heavily laden with dark staining hemosiderin pigment (hemoglobin and hemosiderin ×480). **B**, Gliosis in area outside developing capsule. Dark staining patches represent bundles of glial filaments (glial fibrillary acidic protein ×480). **C**, Reactive astrocytes in surrounding white matter extended for considerable distances from hematoma (glial fibrillary acidic protein ×480). Astrocytic foot processes line walls of blood vessels (*arrow*).

rim of echoes. Late in the capsule stage, fibroblasts began to project into the hematoma center at oblique angles to the encircling capsule. The reticulin stain showed precollagen precursors in this area which contributed further to the thickened echogenic rim. The number of foamy macrophages and fibroblasts in the region immediately next to the hematoma increased (fig. 7D). The perivascular infiltrate on the outer edge of the hemorrhage had regressed and was now composed of foamy macrophages rather than the mononuclear infiltrate noted in the early stages. Hemosiderin was identified only in macrophages. Edema of the white matter continued to resolve while reactive astrocytosis increased in the white matter surrounding the hematoma. Gliosis was seen in the area immediately outside the developing capsule.

The final stage, organization, in the resolution of intracerebral hemorrhage involved removal of the residual hematoma via foamy macrophages, the formation of a dense

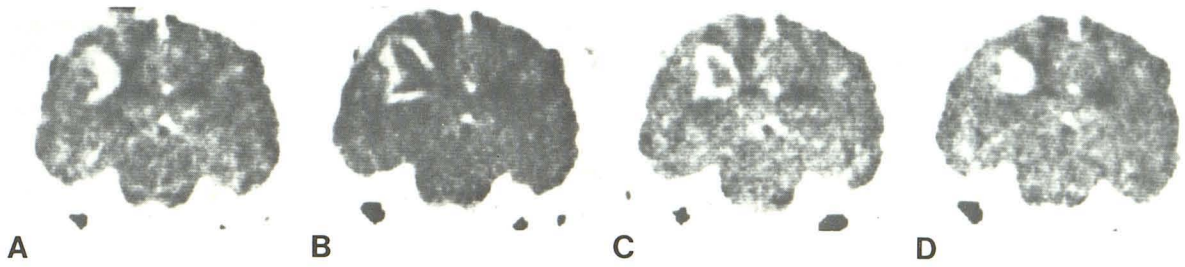

Fig. 10.—Serial coronal CT scans 5 min after bolus of contrast medium correspond to sagittal serial high resolution sonograms in fig. 4. **A**, Day 1. No evident contrast enhancement. **B**, Day 5. Ring contrast enhancement around nearly isodense hemorrhage. Center of ring was kidney-shaped hemorrhage into which contrast never diffused. **C**, Capsule stage, day 9. Ring enhancement, with ring becoming smaller but often thicker on cortical side. Edema partly regressed. **D**, Late capsule and organization stages, day 13. Ring enhancement still smaller but of greater intensity. As neovascularity penetrated the hemorrhage center, contrast enhancement could be detected in center of lesion.

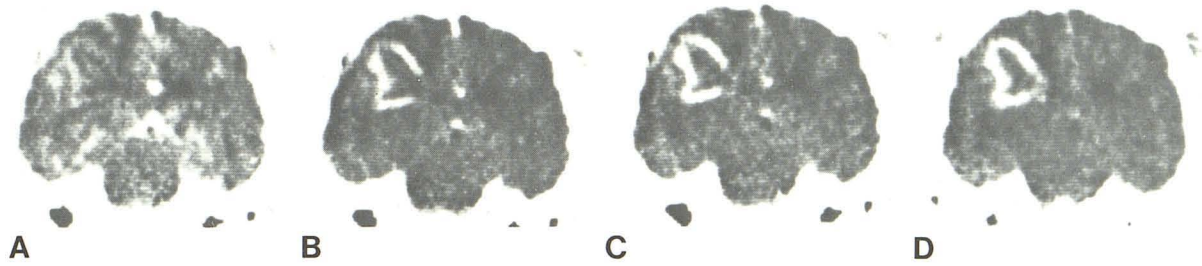

Fig. 11.—Serial coronal CT scans in subacute stage on day 5 at intervals after bolus contrast injection. **A**, Immediately after injection. Enhancement relatively faint. It increased at 5 min (**B**), was maximal at 10 min (**C**), and remained at that intensity for the 30 min scanning period. The ring was often incomplete until 30 min scan (**D**). The isodense central area did not enhance with contrast. No capsule was present at this stage. The two midline punctate areas of enhancement represent vessels that demonstrated steady decrease in blood-iodine level while intensity of ring enhancement around hemorrhage increased or was unchanged.

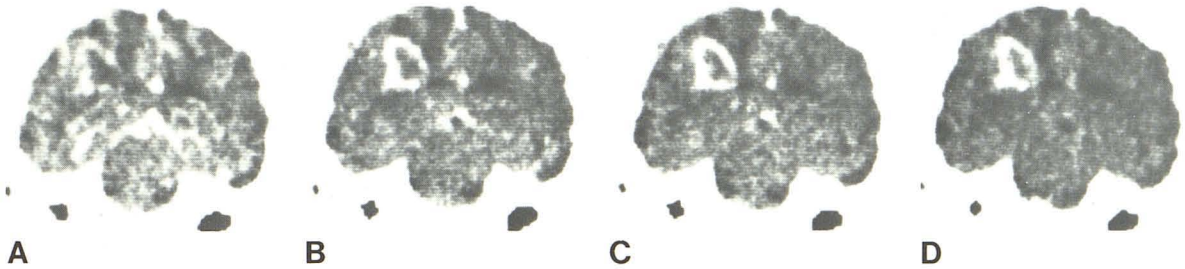

Fig. 12.—Serial coronal CT scans in capsule stage on day 9 at intervals after contrast injection. Immediately (**A**) and 5 min after (**B**) injection. Ring enhancement was smaller compared with subacute stage but still reached peak intensity at 10 min (**C**). However, degree of enhancement began to fade after peak (**D**). Central lucency did not fill in with contrast.

collagenous capsule and the internal organization of the hematoma by a collagenous matrix. Reticulin and collagen stains demonstrated these two separate but related processes. The reticulin and trichrome stains showed the capsule to be comprised of mature collagen running in longitudinal layers around the hematoma (figs. 8A and 8C). In contrast, the process of organization in the center of the hematoma consisted of more random collagen deposition with large numbers of macrophages mixed in (figs. 8B and 8D). These foamy macrophages were densely filled with hemosiderin by the end of the third week (fig. 9A). In this stage, the high resolution sonogram showed further diminution of the hemorrhage with encroachment of echoes into the previously hypoechoic center (figs. 3 and 4). The thickening of the echogenic rim and filling-in of the center reflected the capsule and organization processes. The hemorrhage at this time was difficult to visualize on the noncontrast CT scan because of its small size.

Contrast enhancement on the CT scan first appeared in the subacute stage and took the form of a ring or partial ring outside the actual hemorrhage (fig. 10). Serial CT scans for 30 min after the bolus injection showed no filling of the ring enhancement. The lucent center represented the avascular hematoma into which contrast medium did not diffuse. The intensity of enhancement during the subacute stage reached a peak at 10 min and remained on a plateau for the rest of the 30 min scanning period (figs. 11 and 14). The appearance and location of contrast enhancement corre-

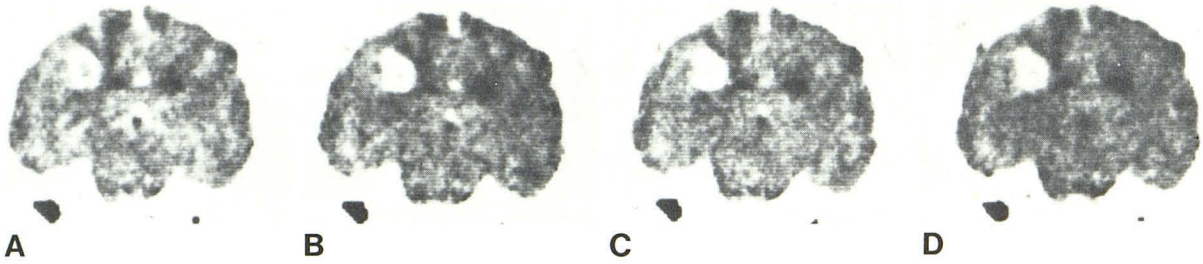

Fig. 13.—Serial coronal CT scans in late capsule and organization stage on day 13 at intervals after bolus contrast injection. Immediately (**A**) and 5 min after (**B**) injection. Peak enhancement at 10 min (**C**) with subsequent fading (**D**). Central lucency filled with contrast in late stages reflecting penetration of hemorrhage center by neovascularity (**D**). Filling occurred only in small, nearly resolved hemorrhages.

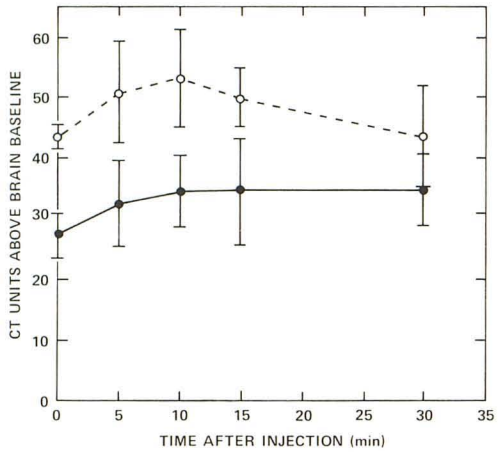

Fig. 14.—Time-density curves of ring contrast enhancement during acute and subacute stages (solid circles, $n = 10$) compared with capsule and organization stages (open circles, $n = 3$). Peak contrast enhancement was detected at 10 min after intravenous bolus injection during both early and late stages. Enhancement was measured as attenuation units above normal brian, which served as baseline and internal control. Plateau was noted after peak during early stages, whereas fading of enhancement occurred during late stages; however, the difference was not statistically significant.

lated most closely to the presence of the mononuclear perivascular infiltrate that encircled the hemorrhage. Developing neovascularity was not prominent and had a similar distribution to the cerebritis.

Ring contrast enhancement on the CT scan continued through the capsule and organization stages of hemorrhage resolution (figs. 12 and 13). The pattern of enhancement retained its ring configuration but its diameter decreased as the hematoma resolved. As long as an avascular residual hematoma remained, a central lucency was identified. Once the central part of the hematoma became vascularized, organized enhancement was nodular. In these late stages, the time-density curve peaked at 10 min and dropped off slowly up to 30 min (figs. 13 and 14). The degree of contrast enhancement was greater compared with the subacute stage, but the difference did not reach statistical significance (fig. 14).

Contrast enhancement on the immediate injection scan (0 min) reflected primarily blood pool iodine and therefore represented vascular structures. This enhancement of vascular structures (cortical vessels and deep venous structures) rapidly faded, as seen on the 10 min scan. In the subacute stage minimal immediate enhancement was noted indicating the minimal presence of neovascularity on the core of the hemorrhage at this stage. As the hemorrhage entered the capsule stage, this immediate enhancement increased reflecting the further proliferation of neovascularity. Again the neovascularity was accented on the cortical side of the hemorrhage but further encircled the hemorrhage. In the late organization stage immediate enhancement had increased to form a full ring indicating formation of neovascularity around the entire resolving hemorrhage. The distribution and the progressive increase in neovascularity from the early capsule stage to the late organizational stage was corroborated histologically.

Discussion

Intracerebral hemorrhage is a relatively common process in many clinical situations. Echoencephalography currently plays a vital role in the recognition of hemorrhage, both subependymal and intraventricular, in premature infants [1–3]. High resolution sonography could play an equally important role in diagnosing and delineating hemorrhage in head trauma [4], postoperative, and brain tumor patients. Therefore, it is important to recognize and understand the sonographic characterization of acute hemorrhage and its pattern of resolution.

Acute hemorrhage stood out in marked echogenic relief to adjacent, normally hypoechoic brain. High resolution sonography accurately defined the size, shape, and location of intracerebral hemorrhage as shown by the CT scan and neuropathologic correlation. However, surrounding cerebral edema was not visualized by sonography. The sonographic appearance of acute hemorrhage was directly related to the integrity of the extravasated red blood cells. Tightly packed collections of intact red blood cells were highly echogenic. This echogenicity decreased as the red blood cells lysed. Red blood cell disintegration occurred first in the center of the hemorrhage causing the appearance of a hypoechoic center. The rim remained echogenic because peripherally located red blood cells remained intact for a longer period of time. The hemorrhage became isodense with surrounding brain on the CT scan as the red blood cells broke down and

lost their hemoglobin. As the hemorrhage passed through this stage, it was often difficult to detect on the noncontrast CT scan while it was still readily detectable on the sonogram by the characteristic echogenic rim–hypoechoic center. In clinical practice it is not unusual for the CT scan to be obtained several days after the onset of subependymal germinal matrix hemorrhage; false-negative CT scans can occur in such instances because the hemorrhage may be isodense at that time and because contrast infusion is not used routinely in these infants.

While the echogenic rim in the early stages of hemorrhage resolution was related primarily to intact red blood cells at the periphery, the peripheral collagen-macrophage network was the key factor in later stages. This echogenic rim thickened as the lesion decreased in diameter reflecting the process of capsule formation and organization of the hemorrhage center. Although we were not able to quantify the difference in echoes by either amplitude or frequency analysis, there is a distinct difference in the character of the echoes caused by red blood cells compared with those caused by the collagen-macrophage network. The latter echoes were less intense and less coarse. Tissue characterization techniques in brain lesion may amplify this distinction. In large, irregular hemorrhages the echogenic and hypoechoic areas may be more complex than the simple ring appearance described for these relatively small hemorrhages. Nevertheless, the pathologic correlates of the source of echoes would be the same.

Contrast enhancement was detected around the periphery of the hemorrhage from the subacute stage onward. In the early stages, the onset and pattern of contrast enhancement correlated best with the presence of the inflammatory mononuclear, perivascular infiltrate at the periphery of the hemorrhage. This correlation was quite similar to the early stages of brain abscess formation (cerebritis stage) in an experimental model where the perivascular infiltrate was much greater and consisted of predominantly polymorphonuclear leukocytes [5]. Perivascular inflammatory cells, whether leaving or entering the vascular space, must traverse the endothelial cell and basement membrane. In doing so they apparently compromise the permeability of the blood-brain barrier to low molecular pharmaceuticals [6]. In both disease processes this perivascular infiltrate is more extensive in the earlier stages as compared with the later stages. The type of cell constituting this perivascular infiltrate also changes with acute inflammatory cells being involved in the earlier stages, whereas macrophages constitute this infiltrate in the later stages. These macrophages remove tissue debris, exit the brain parenchyma, and enter the vascular space, again compromising the blood-brain barrier.

It is interesting that an inflammatory infiltrate appears to be related consistently to the phenomenon of contrast enhancement. This has been shown in widely disparate disease processes: brain abscess, intracerebral hemorrhage, and in zone 2 of adrenoleukodystrophy [7–9]. Only white matter diseases with an inflammatory component have exhibited enhancement with contrast material.

The inflammatory infiltrate appeared concurrently with development of neovascularity. Uptake of radionuclide in an experimental intracerebral hemorrhage model was attributed to this neovascularity, which is believed to have an incomplete blood-brain barrier [10, 11]. In this model, neovascularity was minimal when contrast enhancement was first detected. Although neovascularity could play a role in contrast enhancement in the early stages, it is thought to be minor since data from the brain abscess model showed the inflammatory infiltrate to play a key role in contrast enhancement [5]. The immediate (0 min) scans demonstrated the relative paucity of neovascularity in the subacute stage. In the later stages, this discrepancy decreased. As the hemorrhage matured, cerebritis became less important while increasing capsule neovascularity became predominant in causing contrast enhancement. The transition was gradual. Observations using emission computed tomography have shown increased cerebral blood volume at the periphery of a resolving hematoma [12, 13]. This has been attributed to vasodilation [13]. The proliferation of neovascularity leading to an increased blood volume is a more likely explanation. The greater magnitude of contrast enhancement in the capsule and organization stage compared with the subacute stage suggested a greater breach in the blood-brain barrier. The time-density curves of the early and late stage of both experimental hemorrhage and abscess were remarkably similar reflecting the similar progression of events.

The histologic sequence of changes in capsule formation was quite similar in the experimental hemorrhage and abscess models [5], although the time course was somewhat more rapid in the hemorrhage model. This reflects the limited response of neural tissue to insult. The collagen capsule formed more quickly and more completely on the cortical compared with the ventricular aspect in both lesions. Final resolution was accomplished by vessel and fibroblast invasion of the lesion center from the peripheral capsule.

The high resolution sonographic and CT changes of an evolving intracerebral hemorrhage in our canine series have human counterparts. Although our experimental model of hemorrhage is unrelated to subependymal germinal matrix and intraventricular hemorrhages in the premature infant, the high resolution sonographic appearance of the parenchymal component of this type of neonatal hemorrhage and its temporal changes are remarkably similar [1–3]. The intracerebral hematoma has been shown to diminish by about day 10 in the human adult [12, 14]; this occurred at about day 9 in our model. Perihemorrhage edema has been noted to be maximal around days 2 and 3 [12]; the time course was similar in our series. Contrast enhancement has been reported as early as 3 days postictus in the human, but more often it appears after a week [12, 15]. In our series the contrast enhancement was detected consistently 6 days after placement of hemorrhage but was seen as early as 3 days. The time course of events in the animals seemed shorter compared with the human, probably because of the smaller size of the hemorrhage. However, the sequence of changes was the same.

Indirect evidence of the human counterpart of the inflammatory response observed in this experimental intracerebral hemorrhage has been reported. Elevation of lactoferrin and

lysozyme levels with cerebrospinal fluid occurs in about the same time frame as the appearance of the inflammatory infiltrate [16]. The somewhat greater and longer elevation of lysozyme is consistent with the predominantly monocytic infiltrate. It has been suggested the inflammatory reaction of the brain might exacerbate the insult and thus warrant treatment [16]. This experimental model suggests such treatment may not be worthwhile since the inflammatory infiltrate was not extensive and limited to the immediate area around the hemorrhage. The inflammatory cells were integral to hemorrhage resolution.

At present, high resolution sonographic imaging has a limited role in the radiologist's armamentarium of diagnostic techniques for imaging the brain. A major limitation is access to the area of interest in the intracranial cavity. This is especially true for the high frequency beams required. Nevertheless, further technologic improvement in high resolution scanners promises to expand their use in neuroradiologic practice. In those patients who have acoustical windows in the cranium, such as the neonatal anterior fontanelle or a craniotomy defect from previous surgery, high resolution sonography can be a valuable imaging technique. Intraoperative high resolution sonograms could prove useful in any procedure requiring localization and characterization of a brain lesion. In the new field of hyperthermic treatment of brain tumors where extensive craniotomies may be indicated, high resolution imaging may become an important component in the diagnostic, treatment, and follow-up regimen [17]. Understanding the high resolution appearance of acute hemorrhage and its changing characteristics will be important in fully using high resolution sonography in brain imaging.

ACKNOWLEDGMENTS

We thank Elizabeth Millerman and David Furgassa for histologic preparation of the material; Mary Herman, Division of Neuropathology, for reviewing selected cases; Robert McGowan for performing the glial fibrillary acidic protein stains; Lawrence Eng, Division of Neuropathology, for providing the glial fibrillary acidic protein antisera; and Brigit Mewitz for technical assistance.

REFERENCES

1. London DA, Carroll BA, Enzmann DR. Sonography of ventricular size and germinal matrix hemorrhage in premature infants. *AJNR* **1980**;1:295–300
2. Horbar JD, Walters CL, Philip AGS, Lucey JF. Ultrasound detection of changing ventricular size in posthemorrhagic hydrocephalus. *Pediatrics* **1980**;66:674–677
3. Bejar R, Curbelo V, Coen RW, Leopold G, James H, Gluck L. Diagnosis and follow-up of intraventricular and intracerebral hemorrhages by ultrasound studies of infant's brain through the fontanelles and sutures. *Pediatrics* **1980**;66:661–673
4. Enzmann DR, Britt RH, Lyons B, Buxton TL, Wilson DA. Experimental study of high resolution ultrasound imaging of components of head trauma (hemorrhage, bone fragments and foreign bodies). *J Neurosurg* **1981**; 54:304–309
5. Enzmann DR, Britt RH, Yeager AS. Experimental brain abscess evolution: computed tomographic and neuropathologic correlation. *Radiology* **1979**;133:113–122
6. Fujitz S, Kitamura T. Origin of brain macrophages and the nature of the microglia. In: Zimmerman HM, ed. *Progress in neuropathology*. New York: Grune & Stratton, **1976**:1–50
7. DiChiro G, Eiben RM, Manz HJ, Jacobs IB, Schellinger D. A new CT pattern in adrenoleukodystrophy. *Radiology* **1980**;137:687–692
8. Furuse M, Obayashi T, Tsuji S, Miyatake T. Adrenoleukodystrophy. *Radiology* **1976**;126:707–710
9. Willemse JL, van Dorssen JG, de Haas G, et al. Computerized axial tomography and cerebral scintigraphy in leukodystrophy. *Arch Neurol* **1978**;35:603–607
10. Sugitani Y, Nakama M, Yami Y, Imaizumi M, Nukuda T, Abe H. Neovascularization and increased uptake of ^{99m}Tc in experimentally produced cerebral hematoma. *J Nucl Med* **1973**;14:912–916
11. Di Chiro G, Timins EL, Jones AE, Johnston GS, Hemmock MK, Swann SJ. Radionuclide scanning and microangiography of evolving and completed brain infarction. *Neurology* **1974**;24:418–423
12. Dolinskas CA, Bilaniuk LT, Zimmerman RA, Kuhl DE, Alavi A. Computed tomography of intracerebral hematomas. II. Radionuclide and transmission CT studies of the perihematoma region. *AJR* **1977**;129:689–692
13. Kuhl DE, Alavi A, Hoffman EJ, et al. Local cerebral blood volume in head-injured patients. Determination by emission computed tomography of ^{99}mTc-labeled red cells. *J Neurosurg* **1980**;52:309–320
14. Zimmerman RD, Leeds NE, Naidich TP. Ring blush associated with intracerebral hematoma. *Radiology* **1977**;122:707–711
15. Laster DW, Moody DM, Ball MR. Resolving intracerebral hematoma: alteration of the "ring sign" with steroids. *AJR* **1978**;130:935–939
16. Terent A, Hällgren R, Venge P, Bergström K. Lactoferrin, lysozyme, and β_2-microglobulin in cerebrospinal fluid. *Stroke* **1981**;12:40–46
17. Rubin JM, Mirfakhraee M, Duda EE, Dohrmann GJ, Brown F. Intraoperative ultrasound examination of the brain. *Radiology* **1980**;137:831–832